

A Self-powered Triboelectric Coral-Like Sensor Integrated Buoy for Irregular and Ultra-Low Frequency Ocean Wave Monitoring

Xinyu Wang, Jianhua Liu, Siyuan Wang, Jiayi Zheng, Tangzhen Guan, Xiangyu Liu, Tingyu Wang, Tianyu Chen, Hao Wang, Guangming Xie, Peng Xu,* Jin Tao,* and Minyi Xu*

The design of efficient ocean wave sensors for monitoring the marine environment and revealing dynamic changes has been a major challenge. In this study, a self-powered bionic coral wave sensor (BCWS) based on a triboelectric nanogenerator is proposed. The BCWS captures wave data, which are useful for marine engineering construction, marine resource development, and marine disaster warning. It is mainly composed of triboelectric perceiving units (60 mm in length, 10 mm in width, and 1.5 mm in thickness) encapsulated in coral tentacles, a fixation mechanism, a buoyancy tray, and a counterweight mechanism. With the help of its bio-inspired structural design, the BCWS effectively improves the signal response time and sensitivity in the 3D perception of wave information. In particular, the coral tentacles stimulated by a load cause contact-separation between fluorinated ethylene propylene and conductive ink electrodes, thereby generating electric signals. This analysis of the experimental data reveals that the BCWS perceives wave height, wave frequency, wave period, and wave direction with millimeter accuracy. To demonstrate the applicability and stability of the BCWS, several of its potential functions are illustrated, including controlling light emitting diodes, perceiving wave information in the ocean, and assisting overboard rescue. The results show that the BCWS provides an intelligent solution for modern marine monitoring.

remains a challenge, especially the perception of ocean waves motion.^[1–4] Ocean wave sensing devices based on additional complex mechanical and hydraulic structures typically transform the multi-directional wave motion into linear reciprocation or rotation of these structures to generate electric signals. However, some such devices are restrained by several drawbacks, including lower accuracy and robustness and expensive maintenance costs. Furthermore, impeller-type sensors increase the risk of collision between marine animals,^[5] remote radar sensors impact the lives of marine animals due to the generation of a strong electromagnetic field,^[6] and the laying of large sensing equipment generates noises and disturbances to marine animals^[7] and changes hydrodynamic conditions. Conventional signal processing strategies have been demonstrated to possibly provide insufficient information to estimate ocean wave cues, resulting in difficulty to meet the requirements of high accuracy

(error range in the order of 1 m).^[8,9] Moreover, most of these ocean wave sensors need an external power supply, and the high cost of power supply limits their development. Therefore, novel ocean wave sensing techniques are still an open research topic.

1. Introduction

Ocean motion is closely related to tides, tsunamis, oil and gas resource exploration, and marine biological resource studies. Notably, relatively accurate perception of ocean motion


X. Y. Wang, J. H. Liu, S. Y. Wang, T. Z. Guan, X. Y. Liu, T. Y. Chen,
H. Wang, P. Xu, M. Y. Xu
Marine Engineering College
Dalian Maritime University
Dalian 116026, China
E-mail: pengxu@dlmu.edu.cn; xuminyi@dlmu.edu.cn

J. X. Zheng
Transportation Engineering College
Dalian Maritime University
E-mail: Dalian 116026, China

G. M. Xie
Intelligent Biomimetic Design Lab
College of Engineering
Peking University
Beijing 100871, China

J. Tao
College of Artificial Intelligence
Nankai University
Tianjin 300350, China
E-mail: taoj@nankai.edu.cn

T. Y. Wang
Electronics Engineering and Computer Science College
Dalian Maritime University
Dalian 116026, China

 The ORCID identification number(s) for the author(s) of this article can be found under <https://doi.org/10.1002/admt.202101098>.

DOI: 10.1002/admt.202101098

Ocean waves are characterized by irregular motion, ultra-low frequency vibrations, and long periodicity, which poses great challenges to the development of ocean wave sensors.^[10–13] Triboelectric nanogenerators (TENGs),^[14–20] based on the triboelectrification effect and electrostatic induction,^[21–23] have shown promise in ocean wave sensing. This is because TENGs have many advantages, including low cost, simple structure, lightweight, high power density, and random acquisition of low-frequency vibration energy.^[24–26] In recent studies, TENGs have exhibited impressive performance in self-powered sensing applications.^[27–33] For instance, Xu et al. presented a wave height-perceiving sensor based on liquid–solid TENGs for real-time monitoring of ocean wave height around offshore platforms.^[34] Furthermore, Zhang et al. proposed a highly sensitive ocean wave spectrum sensor, which is 100 times more sensitive than the sensor designed by Xu et al., for sensing ocean wave information such as wave height, wave frequency, and wave length.^[35] A graded energy harvesting triboelectric nanogenerator was proposed for ocean wave graded energy harvesting and condition monitoring by Xu et al.^[36] Wang et al. designed sandwich-like triboelectric nanogenerators for hydrodynamic parameters revealing and energy harvesting.^[37] However, these ocean wave sensors can only effectively obtain information from one direction or within a relatively narrow bandwidth. In an earlier study, it was observed that biomimicry significantly improved the performance of a variety of self-powered sensors.^[38–40] Particularly inspired by mammals in nature, Wang et al. designed a bionic triboelectric whisker sensor that mimics the follicle structure of rats, offering a new tactile sensing

solution for reactive obstacle avoidance and local mapping in unknown environments.^[41,42] A unique elastic structure of a bionic jellyfish TENG was proposed by Chen et al., in which the TENG had high output performance and effectively monitored liquid level fluctuation.^[43]

Based on the findings of the aforementioned studies, suitable bionic structures combined with TENGs may provide a promising solution to ocean wave perception. Coral reefs are structurally complex and biologically diverse,^[44,45] with about 1/4 to 1/3 of all marine organisms living in coral reefs,^[7,46] meaning that corals are integral to the ocean's ecosystems. When part of a coral is subjected to a small external stimuli, it will receive an external signal via its diffused neural system. Many interesting coral-like applications have been developed based on this phenomenon. For instance, a coral-like Au-modified SnSe₂ nanocomposite was designed to increase the perception properties of ammonia gas at room temperature.^[47] Additionally, a coral-like soft robot with electromagnetic actuators was successfully developed.^[48] However, very few coral-like sensors for marine use provide perception of ocean wave motion. Herein, we design an environmentally friendly sensor combining the principle of TENGs and the biomimicry of coral structure.

In this study, we propose a self-powered bionic coral wave sensor (BCWS) based on a TENG for capturing wave information, where the triboelectric perceiving unit is encapsulated in a flexible coral-shaped silicone structure, as shown in **Figure 1b**. Coral, without the neural center, transmits the signal through a diffused neural system. When the coral is exposed to external stimuli, the tentacles will close, and the entire coral will shrink.

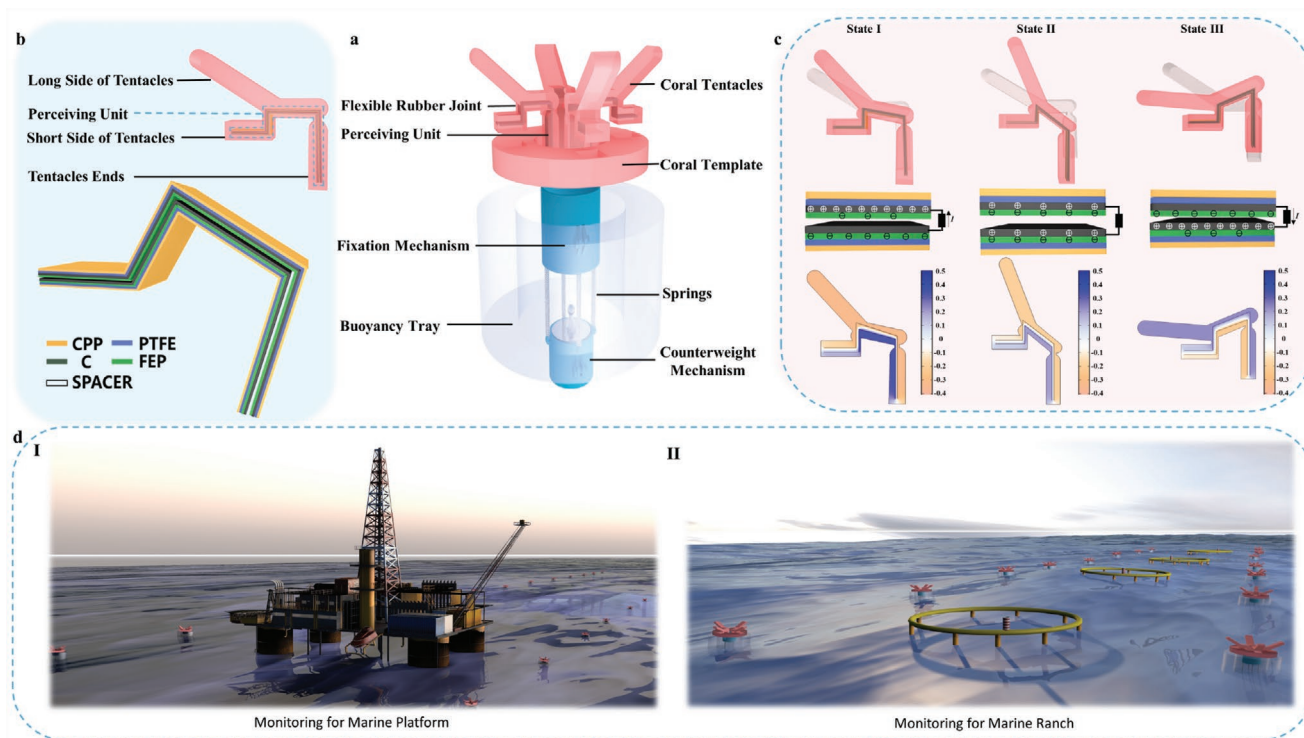


Figure 1. Design, working principle, simulation, and applications of the BCWS. a) The basic structure of the BCWS. b) The detailed structure of the coral tentacle and the perceiving unit. c) i: Movement of the coral tentacle. ii: Schematic charge distribution as the coral tentacle moves. iii Simulation results of the potential distribution between the FEP membrane and conductive ink. d) Applications of the BCWS in the marine platform and marine ranch.

Inspired by the pattern of coral signal transmission via a diffused neural system, we use a nonlinear multi-spring oscillator model for dynamic analysis of wave information considering simple harmonic motion (SHM) in 3D space, as shown in Figure S2, Supporting Information. A counterweight mechanism pulls the tentacles to keep them swinging back and forth for a period, which allows contact-separation motion between fluorinated ethylene propylene (FEP) and conductive ink electrodes in the perceiving units. The output signal generated by the TENG is used to distinguish the magnitude, frequency, and direction of the wave. Finally, we test the BCWS equipped with the acquisition module and wireless transmitter module in the ocean. The test results reveal the sensitivity and accuracy of the BCWS in perceiving wave height, wave frequency, wave period, and wave direction. It is worth noting that the BCWS also demonstrates great potential for overboard rescue due to its sensitivity to load period.

2. Results and Discussion

2.1. Design, Working Principle, and Simulation of BCWS

While floating in the ocean, the BCWS collects the amplitude, direction, frequency, and period of ocean waves. Figure 1a shows the physical structure of the BCWS, which is composed of coral tentacles, a perceiving unit, flexible rubber joints, a coral template, a fixation mechanism, a buoyancy tray, springs, and a counterweight mechanism. The details of the coral tentacles, which mimic tetraploid coral, are shown in Figure 1b. Coral can be classified into tetraploid coral, hexaploid coral, and octoploid coral. By analyzing the experimental results, BCWS with four tentacles has enough capability to obtain ocean wave information. Besides, each tentacle is composed of a long side (60 mm in length, 15 mm in width, and 10 mm in thickness), a short side (15 mm in length, 15 mm in width, and 10 mm in thickness), an end (40 mm in length, 15 mm in width, and 10 mm in thickness), and a perceiving unit (60 mm in length, 10 mm in width, and 1.5 mm in thickness). Together, these components form a double-link mechanism through flexible silicone joints. The short side of tentacles are fixed to the coral template (15 mm in width, 100 mm in diameter) using silicone rubber, which effectively cushions against destructive loads and prevents damage to the sensor. The ends of the tentacles are held together by a fixation mechanism that allows four coral tentacles to oscillate sequentially. The perceiving units of the BCWS, which consist of metalizing cast polypropylene (CPP), polytetrafluoroethylene (PTFE), FEP, and conductive ink electrodes, are shown in Figure 1b. Each perceiving unit is encapsulated in the flexible coral-shaped silicone structure and CPP to reduce the impact of water on sensor performance.^[49] Specifically, silicone rubber structure can avoid direct contact between the perceiving unit and seawater and has anti-corrosion properties that benefit long-period stability. Then, with the help of metalizing cast polypropylene, the exterior of the perceiving units forms an electrostatic shielding layer to reduce the impact of external ions and electrostatic fields on the sensing unit. With the unique encapsulation materials, BCWS can maintain charge density and sensitivity. The long side of each tentacle

swings to make contact with and separate the FEP membrane and the conductive ink electrodes.

The end of the fixation mechanism is connected to the counterweight mechanism with four springs, which can transmit the counterweight mechanism oscillated by a wave motion to the coral tentacles. A spring with the appropriate stiffness coefficient can increase the sensitivity of the BCWS. The counterweight mechanism can adjust the tension of the coral tentacles. If the counterweight is too heavy, the tentacles will not move enough, which will decrease the sensitivity of the BCWS; if the counterweight is too light, the BCWS will not have sufficient resistance to interference from sea wind (Figure S6, Supporting Information). In addition, the coral template is fixed to a buoyancy tray, which provides a suitable floating attitude for the BCWS.

The oscillatory motion and working mechanism of tentacles are illustrated in Figure 1c. The grey coral tentacle model represents the initial position of the coral tentacles. Once the FEP membrane and conductive ink electrodes in the oscillatory motion are in a contact state, the opposite electric charges induced on the surfaces of the two materials overlap via the triboelectric effect. Due to the high electronegativity of FEP compared to conductive ink, it attracts electrons and becomes negatively charged. Meanwhile, the conductive ink loses electrons and becomes positively charged. Then, when the counterweight mechanism and buoyancy tray are in contact with ocean waves, double-link mechanism transmits the force to the tentacle, which drives FEP and conductive ink electrodes to gradually separate with the open coral tentacle. The separation of the FEP membrane and the conductive ink electrode results in a potential difference because the positive and negative charges are no longer on the same plane. Free electrons flow from the FEP film to the conductive ink through an external circuit to balance the potential difference. The flow of free electrons continues until the separation of the two contact surfaces is maximized. The coral tentacles start to close due to the elasticity of the spring when the contact between the counterweight mechanism, buoyancy tray, and ocean wave ends. As a result of inertia, the coral tentacles do not return to the initial position but continue to move downward. During this process, the FEP membrane is pushed back toward the conductive ink electrode with the movement of the coral tentacles. The potential difference decreases during this process, and the free electrons flow back from the conductive ink electrodes to the FEP membrane through the external circuit. Finally, the two surfaces of the conductive ink electrodes and FEP membrane are in contact. The charge distribution returns to its initial state. At this point, the generation of a complete electric power cycle is completed. The working mechanism of the BCWS is further proved by COMSOL software, as shown in Figure 1c. Figure 1d demonstrates two potential applications of the BCWS, wherein multiple BCWSs can be distributed around a marine platform or marine ranch to monitor ocean wave information to indicate safety and stability.

2.2. Output Characterization of the BCWS

For ocean wave information sensors, wave height, wave frequency, wave period, and wave direction are important

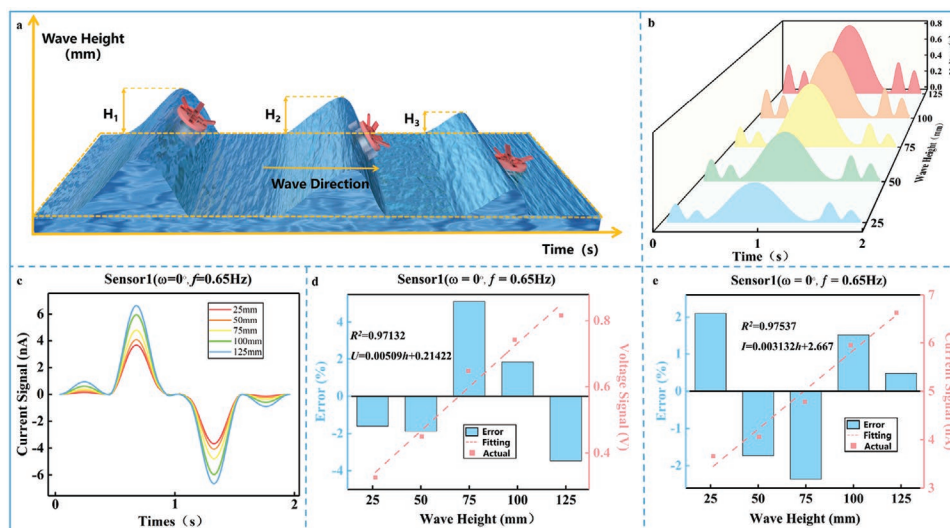


Figure 2. Experimental results. a) Schematic diagram of the BCWS for wave height perception. b) Influence of h on the voltage signal from sensor 1 under the conditions of $\omega = 0^\circ$ and $f = 0.65$ Hz. c) Influence of h on the current signal from sensor 1 under the conditions of $\omega = 0^\circ$ and $f = 0.65$ Hz. d) Leave-one-out cross-validation (LOOCV) for evaluating the accuracy and generalization performance of sensor 1 regarding h and voltage signal. e) LOOCV for evaluating the accuracy and generalization performance of sensor 1 regarding h and current signal.

evaluation indicators. Due to the length limitation of the water tank, the echo waves generated on the wall of the water tank can interfere with the output performance of the BCWS. Thus, we use a swing test bench to simulate various wave heights, wave frequency, wave period, and wave direction, and we use a water tank to simulate the water resistance in a real marine environment, as shown in Figure S1, Supporting Information. Then, in order to describe the experimental results more clearly, we define the wave height, wave frequency, angle, and wave period as h , f , ω , and T . The inset image of Figure S1, Supporting Information, shows the schematic angle diagram of the BCWS. The four sensors are angles coded as 1: 0° , 2: 90° , 3: 180° , and 4: 270° . **Figure 2a** shows the schematic diagram of the BCWS for different wave height perceptions. We take a 1:20 scale of a navigational buoy to fabricate BCWS with the actual ability to perceive ocean wave information. Significantly, the characteristics (wave height and wave period) of the chosen wave conditions at the full scale of the navigational buoy (0.5–2.5 m; 6.5–10 s; 0.1–0.154 Hz) and the same wave conditions converted to the 1:20 scaled BCWS using the Froude similitude law (0.025–0.125 m; 1.45–2.23 s; 0.45–0.67 Hz). Thus, we utilize wave heights from 25 to 125 mm and frequencies from 0.45 to 0.65 Hz to discuss the sensor's performance. **Figure 2b** describes the influence of wave height on the output voltage from sensor 1 when $\omega = 0^\circ$ and $f = 0.65$ Hz. As the wave height increases from 25 to 125 mm, the output voltage signal increases from 0.3255 to 0.8162 V, which demonstrates that the BCWS can effectively sense changes of wave height with millimeter accuracy. Interestingly, two small signals generated by the SHM of the multi-spring system appear on both sides of the main frequency signal. This prolongs the response time, which improves the acquisition module's ability to capture wave signals. In addition, the relationship between the voltage signal and h exhibits excellent linearity, with a correlation coefficient of $R = 0.97132$, as shown in **Figure 2d**. **Figure 2c**

illustrates the influence of wave height on output current when $\omega = 0^\circ$ and $f = 0.65$ Hz. As H increases from 25 to 125 mm, the current signal rises from 3.66 to 6.63 nA. Notably, there is still a small signal in the actual waveform plot of the current signal, which indicates the multi-spring system increases the sensing range and improves the sensitivity of the BCWS. **Figure 2e** shows the linear relationship between wave height and current, with a correlation coefficient of 0.97537.

Furthermore, ocean wave frequencies are also critical parameters for attitude wave information. **Figure 3a** illustrates the perceiving attitude of the BCWS for different ocean wave frequencies. We use the frequency range from 0.45 to 0.65 Hz to simulate ultra-low frequency ocean waves in real ocean conditions. **Figure 3b** shows the influence of wave frequency on output voltage when $\omega = 0^\circ$ and $h = 75$ mm. Surprisingly, as the wave frequency increases from 0.45 to 0.65 Hz, the output voltage signal increases from 0.6248 to 0.6475 V. This is because the acceleration increases with the increasing frequency, resulting in larger inertia of the BCWS and greater motion magnitude of the perceptual unit. Moreover, the linear correlation coefficient between the wave frequency and output voltage is 0.94302, as shown in **Figure 3d**. **Figure 3c** demonstrates that the output current signal gradually increases from 3.2 to 4.78 nA as the wave frequency increases from 0.45 to 0.65 Hz. Due to the increase of frequency, the number of contact separations increases, and the rate of charge transfer becomes faster, leading to an increase in the current signal. **Figure 3e** shows that the frequency and current signals are linear, with a correlation coefficient of 0.9906.

Because obtaining a highly accurate ocean wave period is a significant way to predict marine natural hazards, like storm surges, red tides, and tsunamis, we use wave frequencies to calculate wave period via $T = \frac{1}{f}$. Furthermore, we use the above formula to obtain a theoretical wave period value called theoretical value. Then, we utilize Fourier transform to process the output

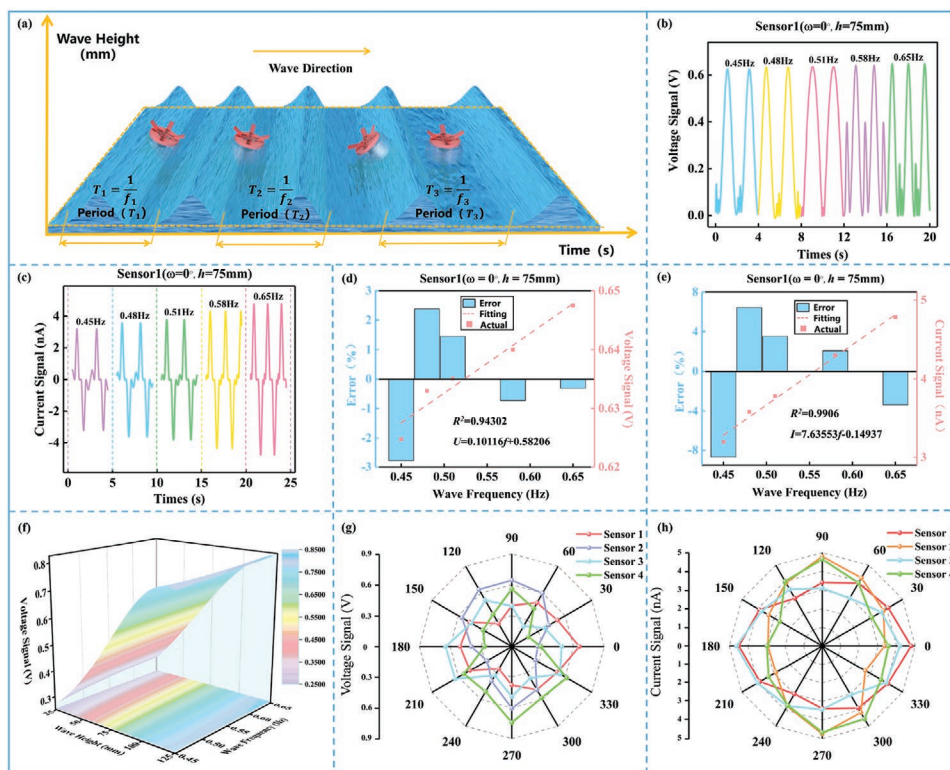


Figure 3. Experimental results. a) Schematic diagram of the BCWS for ocean wave frequency perception. b) Influence of f on the voltage signal from sensor 1 when $\omega = 0^\circ$ and $h = 75$ mm. c) Influence of f on the current signal from sensor 1 when $\omega = 0^\circ$ and $h = 75$ mm. d) LOOCV for evaluating the accuracy and generalization performance of sensor 1 regarding f and voltage signal. e) LOOCV for evaluating the accuracy and generalization performance of sensor 1 regarding f and current signal. f) Influence of h and f on the voltage signal from sensor 1 when $\omega = 0^\circ$. g) Directional patterns of the BCWS in voltage signal. h) Directional patterns of the BCWS in current signal.

signals to obtain the wave period value called measured value. We find that the consistency of theoretical and measured values of the ocean wave period approaches 0.96804, as shown in Figure S2, Supporting Information. Results of humidity, temperature, and durability tests on BCWS are shown in Figures S13– S15, Supporting Information. Notably, under various humidity, temperature, and operation time, the proposed sensor operate stably. The experimental data reveal the high sensitivity and robustness of the BCWS for wave frequency and wave period perception, indicating it can effectively help researchers to make accurate predictions of marine natural disasters.

In order to further illustrate the effects of wave height and wave frequency on the output performance of the BCWS more clearly, Figure 3f shows the relationships among them. It is obvious that when the wave frequency remains constant, the voltage signal gradually increases with the increase of wave height. When the wave height remains constant, the voltage signal increases as the wave frequency increases but at a slower rate compared to the previous condition. This indicates that the wave height has a greater influence on the output of the voltage signal of the BCWS because the degree of contact separation varies more with the increase of wave height. Figure 3g illustrates the influence of angle on the output voltage for sensor 1 under the conditions of $f = 0.65$ Hz and $h = 75$ mm. As the angle increases from 0° to 120° , the voltage signal gradually decreases to 0.257 V. Then the voltage increases to 0.503 V as

the angle increases to 180° . After that, it decreases to 0.254 V from 180° to 240° , and finally increases to 0.51 V from 240° to 330° . Sensors 2, 3, and 4 show the same trend of voltage distribution as sensor 1, showing excellent symmetry and consistency with its own spatial position in Figures S3– S5, Supporting Information. Figure 3h presents the relationship between the angle and the output current. Taking sensor 1 as an example, when the angle increases from 0° to 120° , the current signal gradually decreases from 4.78 to 2.95 nA. Thereafter, as the angle gradually increases to 180° , the current signal increases from 2.95 to 4.49 nA. Then, the current signal decreases to 3 nA from 180° to 240° , and finally increases to 4.08 nA from 240° to 330° . Therefore, the current and voltage signals of the BCWS have a high sensitivity to the angle, allowing the BCWS to effectively sense the direction of ocean waves. We also measure the response time of the proposed BCWS is 45ms, which is shown in Figure S11, Supporting Information. Due to the stability and robustness of the BCWS, it has great value for applications in marine environmental monitoring.

Ocean wave information also includes wave velocity, wavelength, and wave steepness, which can be defined as v , L , and δ . Considering wave velocity first, v can be decomposed into v_v in the vertical direction and v_h in the horizontal direction. Because the buoyancy disk is relatively stationary with the coral template, the speed of the ocean waves only acts on the counterweight mechanism. Furthermore, v_h and the effective

length s acting on the counterweight mechanism are fixed values.^[50] Therefore, we use s , the action time Δt , and the correction factor β to calculate the horizontal velocity as shown in Equation (1).

$$v_h = \frac{s\beta}{\Delta t} \quad (1)$$

Then we use wave height h , action time Δt , and a calibration factor ϵ to calculate the vertical velocity v_v , as shown in Equation (2).

$$v_v = \frac{h\epsilon}{\Delta t} \quad (2)$$

Through the vector synthesis of v_h and v_v , we easily acquire v . Then, we calculate L and δ with the following formulas:

$$L = vT \quad (3)$$

$$\delta = \frac{h}{L} \quad (4)$$

Up to this point, we have obtained almost all wave information through the BCWS. This demonstrates the feasibility of the BCWS to perceive and acquire various wave parameters. Consequently, the BCWS has a promising future due to its comprehensive wave information perception and acquisition.

2.3. Application Demonstration of the BCWS

2.3.1. Real-Time Control Verification

Figure 4a shows the experimental setup of the BCWS connected with a signal sampling module and a trigger signal module. The circuit diagram of their connection is shown in Figure 4b. In this demonstration, we use different magnitudes of stimuli to drive the motion of the tentacles in four directions, which generates electrical pulses to turn on corresponding light emitting diodes (LEDs). Note that there are three LEDs in each direction, and the number of lights depends on the magnitudes of peak voltage signals ranging from 0.5 to 1.5 V (Movie S1, Supporting Information). Taking sensor 2 as an example, Figure 4c indicates the details of the different voltage signals controlling the LED switch on/off. The experiment results reveal that the BCWS has great potential for effectively capturing wave information since it possesses the ability to discriminate the magnitudes of external stimuli based on voltage signals.

2.3.2. Application of BCWS in Real Wave Information Perception

In order to further prove the validity and applicability of the designed BCWS, we test it in a real marine environment. Since the wind and waves in the ocean environment are much larger than in the ideal environment, we fix the BCWS using four

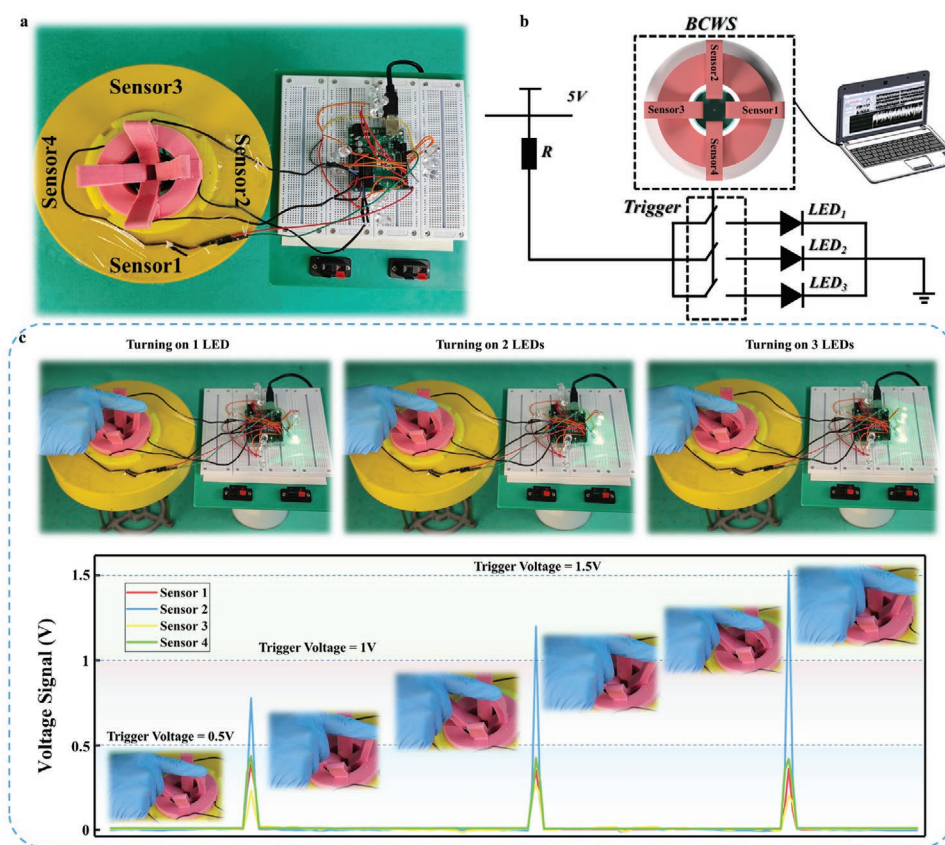


Figure 4. Experimental results. a) Experimental electronic setup. b) Electronic module used for controlling LED lights. c) Demonstration of the BCWS as a load switch control and its corresponding output voltage signal.

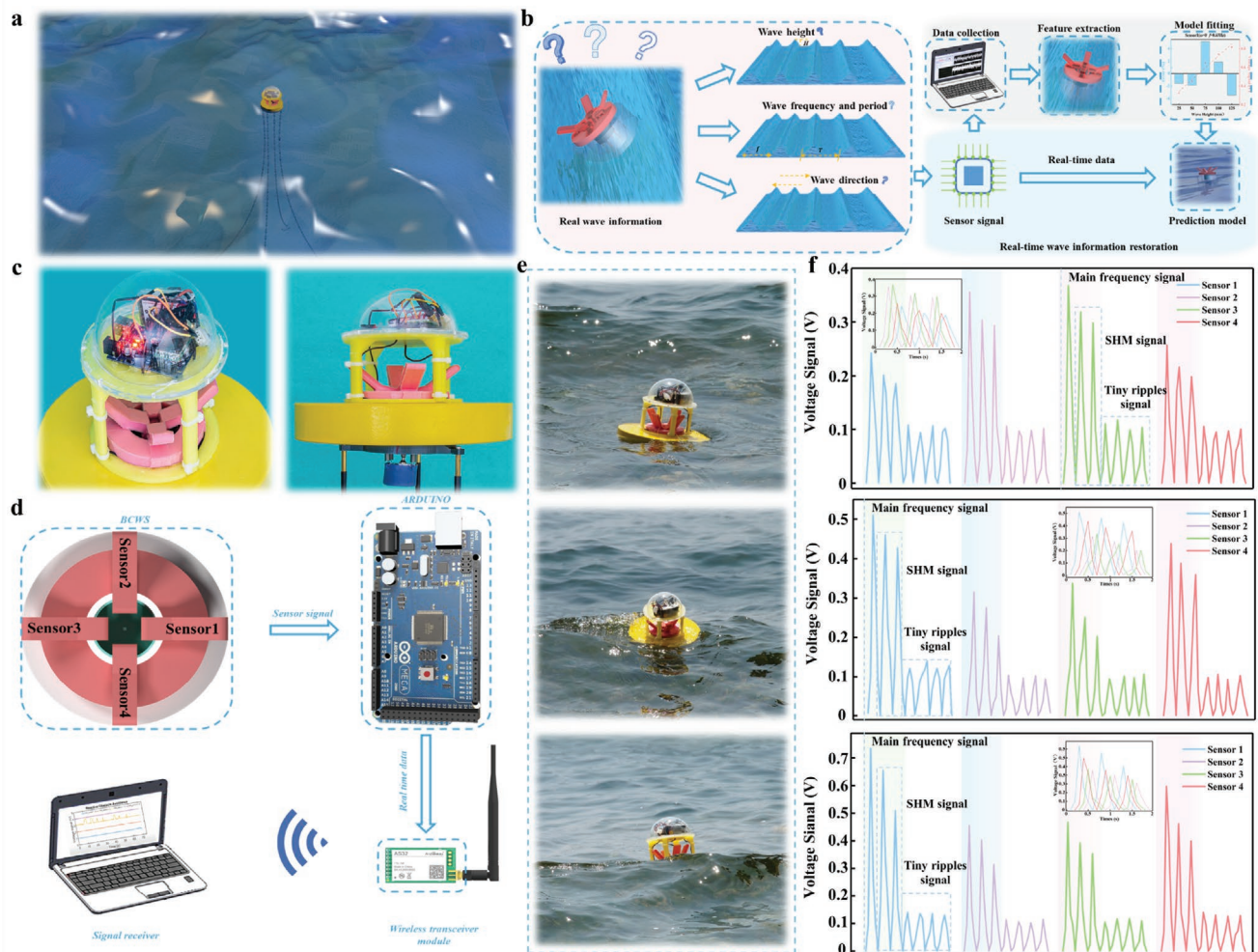


Figure 5. Experimental results. a) Schematic diagram of the BCWS fixed with four anchor chains. b) Real wave information perception process, where sensory information is applied for model fitting and real-time model prediction. c) Photograph of the BCWS equipped with signal processing module and wireless transmission module. d) Schematic diagram of the connection between the BCWS and modules. e, f) Demonstration of the BCWS perceiving various wave information and the corresponding output voltage signals.

anchor chains to prevent it from moving out of place, as shown in Figure 5a. The anchor chains allow the sensor to have little rotation, which would cause a minor influence on perceiving directional load. Figure 5b shows the signal from the BCWS, sampled by module Arduino Mega 2560 and then transmitted to the receiver via the wireless transmission module AS32 TTL 1W. We use an Atmel mega16u2 processor for data processing. The total energy consumption is 4.26 W, including 3.26 W for data acquisition, processing, and 1 W for transmission. Electrostatic shielding wires are used to transmit signals from BCWS. Specifically, the function of electrostatic shielding wires is to exclude electromagnetic waves from a volume of space by enclosing copper nets, called the electrostatic shielding effect. With the help of the electrostatic shielding effect, interference between the signals from different channels is effectively shielded. Then, we use the collected data for model fitting and feature extraction to obtain wave height, wave frequency, wave period, and wave direction, and finally, we construct a prediction model of ocean waves.

Figure 5c shows the photograph of the BCWS equipped with a signal processing module and a wireless transmission module. The signal processing module and wireless transmission module, powered by a 3.3 V lithium battery, can transmit the sampling signal from the BCWS in real time. The schematic diagram of the connection between the BCWS and the signal processing module and the wireless transmission module is shown in Figure 5d. Figure 5e demonstrates the attitude of the BCWS to wave information perception in a real ocean environment. As wave magnitude increases, the BCWS operates normally without capsizing with the aid of the four anchor chains. The processed data of wave information perception are shown in Figure 5f. Specifically, the data from the BCWS include the main frequency signal, SHM signal, and tiny ripples signal. The main frequency signal reveals the information of real waves in real time. Meanwhile, with the help of the SHM signal, the response time is extended, which simplifies the capture of the wave signal by the acquisition module. It is worth noting that the four sensors of the BCWS have different response times for

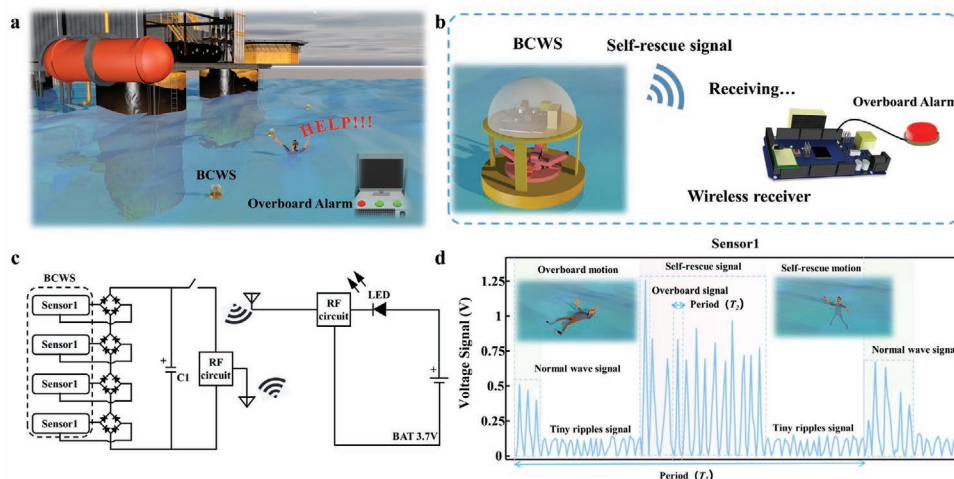


Figure 6. Experimental results. a) Schematic diagram of the BCWS and alarm applied in overboard rescue. b) Schematic of the signal transmission between the BCWS and the alarm. c) Electronic module used for overboard rescue. d) Demonstration of the difference between the wave signal and self-rescue action signal.

the same wave, and there is a certain sequence of their movements (Movie S2, Supporting Information), which is shown in the inset image of Figure 5f. Therefore, the direction of the waves can be effectively determined by the response time. Wave information such as wave height, wave frequency, wave period, and wave direction can be obtained through data processing and signal analysis (Movie S2, Supporting Information). This demonstration shows the feasibility of using the BCWS for constructing a marine environmental monitoring system with low cost and accurate sensing.

2.3.3. Application of the BCWS in Overboard Rescue

Marine platforms and ranches are relatively isolated places. Once a platform staff falls into the water, the ocean environment makes it difficult to find these drowning people. At the same time, because these working staffs are scattered on the platforms, suddenly one missing person cannot be noticed for a short time. In particular, people falling into the water caused by platform tilting accidents are extremely difficult to rescue. The BCWS can effectively sense when a person falls into the water. The diagram of the BCWS applied to overboard rescue is shown in Figure 6a. Once person falls into the water, they use their limbs to perform self-rescue actions, such as swim or attempt to swim, on the surface of water. The BCWS will receive self-rescue action signals intermingled with wave signals. The diagram of signal transmission is presented in Figure 6b. The circuit diagram of the connection is presented in Figure 6c. However, due to the long periodicity characteristics of seawater, the period of self-rescue signal is much smaller than the normal wave signal. The detailed data are shown in Figure 6d, which indicates the difference between the normal wave signal and the self-rescue action signal. Notably, there is an unusually large overboard signal once a person falls into the water. Then, a series of self-rescue signals appear, with a much smaller period than the period of waves. When the sampling

signal of the BCWS suddenly has an abnormally small period, an alarm will sound in the marine platform or marine ranch (Movie S3, Supporting Information), and a rescuer will know where to find the fallen person according to the location of the sensor. The prototype of the BCWS-based rescue system shows great value in creating a novel method for alerting to overboard people.

3. Conclusion

In this study, we propose a bionic coral wave sensor based on TENGs. The BCWS is a sensor combining the principle of TENG and the biomimicry of coral structure, which allows it to possess many advantageous characteristics, such as high sensitivity, high stability, nonlinear multi-spring oscillator model motions, and environmental friendliness. We determine the law of sensor induction from the experimental data, and we establish the data analysis model through experimental research and analysis. Due to the high accuracy and robustness of the BCWS, it can realize 3D wave information sensing in any direction without external energy supply, and the wave information can be collected into the visualization user interface developed based on Arduino Mega 2560. Furthermore, the sensor can predict wave information within a certain distance. With the capabilities of real-time 3D wave information sensing and wave information prediction, there is no doubt that the novel scheme of the BCWS holds great promise for marine engineering monitoring.

4. Experimental Section

Fabrication of the BCWS: The BCWS consisted of coral tentacles, flexible rubber joints, a coral template, a perceiving unit, a fixation mechanism, a buoyancy tray, springs, and a counterweight mechanism. The coral tentacle was made of Dragonskin FX-Pro. Dragon skin FX-Pro is compliant with ISO 10993-10-Biological assessment of medical

facilities, meaning that materials of the sensor are less damaged to the marine environment. Specifically, 12 mL part A and 12 mL part B of silicone rubber were mixed in a petri dish. Then, a vacuum pump was used to vacuum the mixture to -0.1 MP for 2.5 min. When the evacuation of the mixture was complete, the mixture was poured into the female mold, which had been manufactured by 3D printing. The female mold had two joint grooves and a slot in which to manufacture a double-link mechanism and set the perceiving unit. After the liquid silicone rubber was solidified, two silicone rubber joints formed with joint grooves. A double-link mechanism was already manufactured with long-side, short-side, end of the tentacle, and two silicone rubber joints. The perceiving unit was made of CPP, PTFE, FEP, and conductive ink electrodes (60 mm in length, 10 mm in width, and 1.5 mm in thickness). The conductive ink was No. CH-8 (MOD2) produced by JUJO printing supplies technology (Pinghu) Co. Ltd. A 1.5 mm misplacement between FEP and conductive ink electrodes could create air gaps among the membranes. After 30 h solidification at 25 °C, half of the perceiving unit was encapsulated with silicone rubber in the female mold. Then, the semi-encapsulated perceiving unit was put into the male mold for secondary encapsulation. Finally, a complete coral tentacle was obtained. The coral template was filled with 50 mL of silicone rubber. The buoyancy tray was composed of painted polyurethane foam. The fixation mechanism and counterweight mechanism were fabricated by 3D printing. The fixation mechanism and the end of the coral tentacle were fixed by silicone gel. On the bottom of the fixation mechanism, four holes were included to attach the springs. The ends of the springs were connected to the counterweight mechanism, which could be adjusted to different weights.

Measurement System: The output electric signals (open-circuit voltage and short-circuit current) of the BCWS were measured by a programmable electrometer (Keithley 6514), and a data acquisition (DAQ) board (National Instruments, DAQ-9174) was used for data acquisition. The real wave signal from the BCWS was sampled by module Arduino Mega 2560 and then transmitted to the computer through the wireless transmission module AS32 TTL 1W. The COMSOL Multiphysics software was used to simulate the potential electrical distribution of the BCWS.

Supporting Information

Supporting Information is available from the Wiley Online Library or from the author.

Acknowledgements

X.Y.W., J.H.L. and S.Y.W. contributed equally to this work. The authors would like to thank the National Natural Science Foundation of China (Grant Nos. 51879022, 91648120, 61633002, 51575005, 61503008, and 62003175), the Beijing Natural Science Foundation (No. 4192026), the Fundamental Research Funds for the Central Universities (Grants Nos. 3132019037 and 3132019197), and the Academy of Finland (Grant No. 315660).

Conflict of Interest

The authors declare no conflict of interest.

Statistical Analysis

Data are given as mean \pm se. Estimates of statistical significance are performed by Anova (Tukey test, SigmaStat software), values of $p < 0.05$ being considered significant.

Data Availability Statement

The data that support the findings of this study are available from the corresponding author upon reasonable request.

Keywords

bionic wave sensor, multi-spring oscillator model, ocean wave monitoring, self-powered sensors, triboelectric nanogenerators

Received: August 25, 2021

Revised: October 30, 2021

Published online:

- [1] P. Harris, A. Heap, S. Bryce, R. Porter-Smith, D. Ryan, D. Heggie, *J. Sediment. Res.* **2002**, *72*, 858.
- [2] I. Grevemeyer, R. Herber, H.-H. Essen, *Nature* **2000**, *408*, 349.
- [3] F. Ardhuin, L. Gualtieri, E. Stutzmann, *Geophys. Res. Lett.* **2015**, *42*, 765.
- [4] B. Gaylord, M. W. Denny, M. A. Koehl, *Limnol. Oceanogr.* **2003**, *48*, 860.
- [5] L. Xu, T. Jiang, P. Lin, J. J. Shao, C. He, W. Zhong, X. Y. Chen, Z. L. Wang, *ACS Nano* **2018**, *12*, 1849.
- [6] O. Emmanuel, J. Ruscoe, J. Side, R. Harris, S. Kerr, C. Bullen, *J. Oceanogr. Mar. Sci.* **2010**, *1*, 1001.
- [7] J. P. Dinh, J. J. Suca, A. Lillis, A. Apprill, J. K. Llopiz, T. A. Mooney, *Mar. Pollut. Bull.* **2018**, *136*, 282.
- [8] C. Wang, Q. Li, Y. Liu, G. Wu, P. Liu, X. Ding, *ISPRS J. Photogramm. Remote Sens.* **2015**, *101*, 22.
- [9] C. Calkoen, G. Hesselmann, G. Wensink, J. Vogelzang, *Int. J. Remote Sens.* **2001**, *22*, 2973.
- [10] M. Xu, T. Zhao, C. Wang, S. L. Zhang, Z. Li, X. Pan, Z. L. Wang, *ACS Nano* **2019**, *13*, 1932.
- [11] Z. L. Wang, *Nat. News* **2017**, *542*, 159.
- [12] X. Wang, Z. Wen, H. Guo, C. Wu, X. He, L. Lin, X. Cao, Z. L. Wang, *ACS Nano* **2016**, *10*, 11369.
- [13] Z. Wen, H. Guo, Y. Zi, M.-H. Yeh, X. Wang, J. Deng, J. Wang, S. Li, C. Hu, L. Zhu, Z. L. Wang, *ACS Nano* **2016**, *10*, 6526.
- [14] X. Zhang, M. Yu, Z. Ma, H. Ouyang, Y. Zou, S. L. Zhang, H. Niu, X. Pan, M. Xu, Z. Li, Z. L. Wang, *Adv. Funct. Mater.* **2019**, *29*, 1900327.
- [15] X. Xiao, X. Zhang, S. Wang, H. Ouyang, P. Chen, L. Song, H. Yuan, Y. Ji, P. Wang, Z. Li, M. Xu, Z. L. Wang, *Adv. Energy Mater.* **2019**, *9*, 1902460.
- [16] H. Zhao, X. Xiao, P. Xu, T. Zhao, L. Song, X. Pan, J. Mi, M. Xu, Z. L. Wang, *Adv. Energy Mater.* **2019**, *9*, 1902824.
- [17] T. Jin, Z. Sun, L. Li, Q. Zhang, M. Zhu, Z. Zhang, G. Yuan, T. Chen, Y. Tian, X. Hou, C. Lee, *Nat. Commun.* **2020**, *11*, 5381.
- [18] M. Xu, P. Wang, Y.-C. Wang, S. L. Zhang, A. C. Wang, C. Zhang, Z. Wang, X. Pan, Z. L. Wang, *Adv. Energy Mater.* **2018**, *8*, 1702432.
- [19] M. Pan, C. Yuan, X. Liang, J. Zou, Y. Zhang, C. Bowen, *iScience* **2020**, *23*, 101682.
- [20] L. Jin, B. Zhang, L. Zhang, W. Yang, *Nano Energy* **2019**, *66*, 104086.
- [21] Z. L. Wang, T. Jiang, L. Xu, *Nano Energy* **2017**, *39*, 9.
- [22] Y. Fang, T. Tang, Y. Li, C. Hou, F. Wen, Z. Yang, T. Chen, L. Sun, H. Liu, C. Lee, *iScience* **2021**, *24*, 102300.
- [23] C. Rodrigues, M. Ramos, R. Esteves, J. Correia, D. Clemente, F. Gonçalves, N. Mathias, M. Gomes, J. Silva, C. Duarte, T. Morais, P. Rosa Santos, F. Taveira Pinto, A. Pereira, J. Ventura, *Nano Energy* **2021**, *84*, 105890.
- [24] K. Venugopal, P. Panchatcharam, A. Chandrasekhar, V. Shanmugasundaram, *ACS Sens.* **2021**, *6*, 1681.
- [25] W.-G. Kim, D.-W. Kim, I.-W. Tcho, J.-K. Kim, M.-S. Kim, Y.-K. Choi, *ACS Nano* **2021**, *15*, 258.
- [26] A. Ahmed, I. Hassan, A. S. Helal, V. Sencadas, A. Radhi, C. K. Jeong, M. F. El-Kady, *iScience* **2020**, *23*, 101286.

- [27] S. Wang, Y. Wang, D. Liu, Z. Zhang, W. Li, C. Liu, T. Du, X. Xiao, L. Song, H. Pang, M. Xu, *Sens. Actuators, A* **2021**, 317, 112459.
- [28] H. Chen, C. Xing, Y. Li, J. Wang, Y. Xu, *Sustainable Energy Fuels* **2020**, 4, 1063.
- [29] H. Chen, Y. Song, X. Cheng, H. Zhang, *Nano Energy* **2019**, 56, 252.
- [30] H. Guo, X. Pu, J. Chen, Y. Meng, M.-H. Yeh, G. Liu, Q. Tang, B. Chen, D. Liu, S. Qi, C. Wu, C. Hu, J. Wang, Z. L. Wang, *Sci. Robot.* **2018**, 3, eaat2516.
- [31] Y. Liu, E. Li, X. Wang, Q. Chen, Y. Zhou, Y. Hu, G. Chen, H. Chen, T. Guo, *Nano Energy* **2020**, 78, 105403.
- [32] A. Ahmed, Z. Saadatnia, I. Hassan, Y. Zi, Y. Xi, X. He, J. Zu, Z. L. Wang, *Adv. Energy Mater.* **2017**, 7, 1601705.
- [33] X. Pu, S. An, Q. Tang, H. Guo, C. Hu, *iScience* **2021**, 24, 102027.
- [34] M. Xu, S. Wang, S. L. Zhang, W. Ding, P. T. Kien, C. Wang, Z. Li, X. Pan, Z. L. Wang, *Nano Energy* **2019**, 57, 574.
- [35] C. Zhang, L. Liu, L. Zhou, X. Yin, X. Wei, Y. Hu, Y. Liu, S. Chen, J. Wang, Z. L. Wang, *ACS Nano* **2020**, 14, 7092.
- [36] Y. Xu, W. Yang, X. Lu, Y. Yang, J. Li, J. Wen, T. Cheng, Z. L. Wang, *ACS Nano* **2021**, 15, 16368.
- [37] H. Wang, Z. Fan, T. Zhao, J. Dong, S. Wang, Y. Wang, X. Xiao, C. Liu, X. Pan, Y. Zhao, M. Xu, *Nano Energy* **2021**, 84, 105920.
- [38] Y. Zou, P. Tan, B. Shi, H. Ouyang, D. Jiang, Z. Liu, H. Li, M. Yu, C. Wang, X. Qu, et al., *Nat. Commun.* **2019**, 10, 1.
- [39] F. Wang, Z. Ren, J. Nie, J. Tian, Y. Ding, X. Chen, *Adv. Mater. Technol.* **2020**, 5, 1900789.
- [40] X. Li, C. Jiang, F. Zhao, Y. Shao, Y. Ying, J. Ping, *Nano Energy* **2020**, 73, 104738.
- [41] X. Wang, P. Xu, Z. Ma, S. Wang, G. Xie, M. Xu, in *2020 35th Youth Academic Annual Conf. of Chinese Association of Automation (YAC)*, IEEE, Piscataway, NJ **2020**, pp. 105–109.
- [42] P. Xu, X. Wang, S. Wang, T. Chen, J. Liu, J. Zheng, W. Li, M. Xu, J. Tao, G. Xie, *Research* **2021**, 2021.
- [43] B. D. Chen, W. Tang, C. He, C. R. Deng, L. J. Yang, L. P. Zhu, J. Chen, J. J. Shao, L. Liu, Z. L. Wang, *Mater. Today* **2018**, 21, 88.
- [44] C. Ferrier-Pagès, M. C. Leal, R. Calado, D. W. Schmid, F. Bertucci, D. Lecchini, D. Allemand, *Mar. Pollut. Bull.* **2021**, 165, 112129.
- [45] N. Knowlton, *Proc. Natl. Acad. Sci. USA* **2001**, 98, 5419.
- [46] I. Vanwonderghem, N. S. Webster, *iScience* **2020**, 23, 100972.
- [47] Q. Pan, T. Li, D. Zhang, *Sens. Actuators, B* **2021**, 332, 129440.
- [48] N. Kohls, I. Abdeally, B. P. Ruddy, Y. C. Mazumdar, *ASME Lett. Dyn. Syst. Control* **2021**, 1, 031011.
- [49] S. L. Zhang, M. Xu, C. Zhang, Y.-C. Wang, H. Zou, X. He, Z. Wang, Z. L. Wang, *Nano Energy* **2018**, 48, 421.
- [50] T. Isse, D. Suetsugu, H. Shiobara, H. Sugioka, K. Yoshizawa, T. Kanazawa, Y. Fukao, *Geophys. Res. Lett.* **2006**, 33, 16.